Mon. Not. R. Astron. Soc. **000**, 1–22 (—-) Printed 7 April 2010 (MN LATEX style file v1.4)

Effects of the integrated galactic IMF on the chemical evolution of the solar neighbourhood

F. Calura[1,2⋆], S. Recchi[3], F. Matteucci[1,2], P. Kroupa[4]

(1) Dipartimento di Astronomia-Universitá di Trieste, Via G.B. Tiepolo 11, 34131 Trieste, Italy
(2) INAF, Osservatorio Astronomico di Trieste, via G.B. Tiepolo 11, 34131 Trieste, Italy
(3) Institute of Astronomy, Vienna University, Türkenschanzstrasse 17, A-1180, Vienna, Austria
(4) Argelander Institute for Astronomy, Bonn University, Auf dem Hügel 71, 53121 Bonn, Germany

Accepted —- . Received —- ; in original form —-

ABSTRACT

The initial mass function determines the fraction of stars of different intial mass born per stellar generation. In this paper, we test the effects of the integrated galactic initial mass function (IGIMF) on the chemical evolution of the solar neighbourhood. The IGIMF (Weidner & Kroupa 2005) is computed from the combination of the stellar intial mass function (IMF), i.e. the mass function of single star clusters, and the embedded cluster mass function, i.e. a power law with index β. By taking into account also the fact that the maximum achievable stellar mass is a function of the total mass of the cluster, the IGIMF becomes a time-varying IMF which depends on the star formation rate. We applied this formalism to a chemical evolution model for the solar neighbourhood and compared the results obtained by assuming three possible values for β with the results obtained by means of a standard, well-tested, constant IMF. In general, a lower absolute value of β implies a flatter IGIMF, hence a larger number of massive stars and larger metal ejection rates. This translates into higher type Ia and II supernova rates, higher mass ejection rates from massive stars and a larger amount of gas available for star formation, coupled with lower present-day stellar mass densities. Lower values of β correspond also to higher metallicities and higher [α/Fe] values at a given metallicity. We consider a large set of chemical evolution observables and test which value of β provides the best match to all of these constraints. We also discuss the importance of the present day stellar mass function (PDMF) in providing a way to disentangle among various assumptions for β. Our results indicate that the model adopting the IGIMF computed with $\beta \simeq 2$ should be considered the best since it allows us to reproduce the observed PDMF and to account for most of the chemical evolution constraints considered in this work.

Key words: Galaxy: interstellar medium; Galaxies: evolution; Galaxies: abundances; Galaxies: star clusters.

1 INTRODUCTION

The initial stellar mass function is one of the major ingredients of chemical evolution models. Moreover, observed chemical abundances allow one to put robust constraints on both the normalization and the slope of the initial mass function (IMF; Chiappini et al. 2000; Romano et al. 2005). The environment providing most observational constraints for chemical evolution studies is the solar neighbourhood (S. N. hereinafter), for which a large set of observables are available. These observables include diagrams of abundance ratios versus metallicity, particularly useful when they involve two elements synthesised by stars on different timescales. An example is the [α/Fe] vs [Fe/H] diagram, since α elements are produced by massive stars on short (< 0.03 Gyr) timescales, while type Ia supernovae (SNe) produce mostly Fe on timescales spanning from 0.03 Gyr up to one Hubble time (Matteucci 2001). This diagnostic is a strong function of the IMF, but depends also on the assumed star formation history (Matteucci 2001; Calura et al. 2009). Another fundamental constraint is the metallicity distribution of living stars, which provides us with fundamental information on the IMF and on the infall history of the studied system. Another diagnostic, depending both on the IMF and the past star formation history, is the present-day mass function, which represents the mass function of living stars ob-

⋆ E-mail: fcalura@oats.inaf.it

served now in the Solar Vicinity (Elmegreen & Scalo 2006). Other important observables useful for chemical evolution studies include the type Ia and type II SN rates, as well as the surface density of stars and gas, depending on the IMF and on the rate at which the gas has been processed into stars and remnants in the past, i.e. on the SFR.

In a previous paper, Recchi et al. (2009) considered a star-formation dependent IMF, called the integrated galactic initial mass function (IGIMF), which originates from the combination of the stellar IMF within each star cluster and the embedded cluster mass function. † Within each star cluster, the IMF can be well approximated by a two-part power-law form, $\xi(m) \propto m^{-\alpha}$ (e.g. Pflamm-Altenburg, Weidner & Kroupa 2007). Massey & Hunter (1998) have shown that for stellar masses $m >$ a few $M_\odot$, a slope similar to the Salpeter (1955) index (i.e. $\alpha = 2.35$) can approximate well the IMF in clusters and OB associations for a wide range of metallicities. Other studies have shown that the IMF flattens out below $m \sim 0.5$ $M_\odot$ (Kroupa, Tout & Gilmore 1993; Chabrier 2003). On the other hand, the embedded cluster mass function is well approximated by a single slope power law. This implies that small embedded clusters are more numerous in galaxies and they lock up most of of the stellar mass. However, the most massive stars tend to form preferentially in massive clusters (Weidner & Kroupa 2006). The integrated IMF in galaxies, the IGIMF, is a function of the galactic star formation rate (SFR) and, as a consequence of the embedded cluster mass function, it is steeper than the stellar IMF within each single star cluster (Kroupa & Weidner 2003; Weidner & Kroupa 2005).

Recchi et al. (2009) studied the effects of the IGIMF on the evolution of the SN rates in galaxies and on the chemical evolution of elliptical galaxies, showing how the IGIMF naturally accounts for the relation between the [α/Fe] and the stellar velocity dispersion observed in local elliptical galaxies. In this paper, we consider the effects of the IGIMF on the chemical evolution of the solar neighbourhood. As already stressed, the advantage of this approach is the availability of a large set of observational constraints, useful to test the IGIMF and, most importantly, to constrain its main parameter, i.e. the index β of the power law expressing the embedded clusters mass function.

We will compare the results computed by means of a standard IMF, similar to the one by Scalo (1986), successful in reproducing most of the chemical evolution properties of the Solar Neighbourhood, with the results computed by means of the IGIMF. This Paper is organized as follows. In Section 2 we describe the IMF used in standard chemical evolution models and the formalism behind the IGIMF. In Section 3 we present a brief description of the chemical evolution model of the Solar Neighbourhood. In Sect. 4 we present our results and in Sect. 5 we draw our conclusions.

† Embedded clusters are stellar clusters that are partially or fully encased in interstellar gas and dust within molecular clouds, therefore often visible only in the infrared. It is supposed that all (or the large majority of) the stars form originally in embedded clusters (Lada & Lada 1991), but then they can loose their cocoon of gas because of the feedback of O stars (see e.g. Boily & Kroupa 2003a,b). We will name therefore hereafter "embedded clusters" also the clusters which have lost their envelope, but still retain all of their stars, to be consistent with the terminology used in the original papers describing the IGIMF theory (e.g. Kroupa & Weidner 2003; Weidner & Kroupa 2005).

2 THE INITIAL MASS FUNCTION

2.1 The standard initial mass function

$\xi_{std}(m)$ is the initial mass function assumed in the standard chemical evolution model used in this paper and is a two-slope power law, defined in number as:

$$\xi_{std}(m) = \begin{cases} 0.19 \cdot m^{-2.35} & \text{if } m < 2\,M_\odot \\ 0.24 \cdot m^{-2.70} & \text{if } m > 2\,M_\odot, \end{cases} \quad (1)$$

In the remainder of the paper, we will refer to the IMF of Eq. 1 as to the *Standard* IMF. This equation represents a simplified two-slope approximation of the actual Scalo (1986) IMF, similarly to what is done in Matteucci & François (1989). Our basic IMF is assumed to be constant in space and time and normalized in mass to unity in the mass interval $0.1 - 100 M_\odot$, i.e.:

$$\int m \xi_{std}(m) dm = 1. \quad (2)$$

Various papers have shown that, by assuming this IMF it is possible to reproduce a large number of observational constraints for the solar neighbourhood (Chiappini et al. 2001; Romano et al. 2005). By means of our chemical evolution model, we will present predictions for various observables computed by assuming the standard IMF. These predictions will be tested against observed quantities and will be compared to results computed assuming the integrated galactic IMF, which is the subject of the following section.

2.2 The integrated galactic initial mass function

The IGIMF theory has been described in detail in previous papers (Kroupa & Weidner 2003; Weidner & Kroupa 2005; Recchi, Calura & Kroupa 2009). Here we briefly summarize its main assumptions and features. The IGIMF theory is based on the assumption that all the stars in a galaxy form in star clusters. Within each embedded cluster, the stellar IMF has the canonical form $\xi(m) = k m^{-\alpha}$, with $\alpha = 1.3$ for ~ 0.1 $M_\odot \leq m < 0.5$ $M_\odot$ and $\alpha = 2.35$ (i.e. the Salpeter slope) for 0.5 $M_\odot \leq m < m_{\rm max}$. The upper mass $m_{\rm max}$ depends on the mass of the embedded cluster $M_{\rm ecl}$ simply because small clusters do not have enough mass to produce very massive stars.

On the other hand, star clusters are also apparently distributed according to a single-slope power law, $\xi_{\rm ecl} \propto M_{\rm ecl}^{-\beta}$ (Zhang & Fall 1999; Lada & Lada 2003). In this work we have assumed 3 possible values of β: 1.00, 2.00 and 2.35 . By convolving the stellar IMF with the distribution of embedded clusters we obtain the IGIMF, namely the IMF integrated over the whole population of embedded clusters forming in a galaxy as a function of the star formation rate $\psi(t)$:

$$\xi_{\rm IGIMF}(m;\psi(t)) = \int_{M_{\rm ecl,min}}^{M_{\rm ecl,max}(\psi(t))} \xi(m \leq m_{\rm max}) \xi_{\rm ecl}(M_{\rm ecl}) dM_{\rm ecl}, \quad (3)$$

where $M_{\rm ecl,min}$ and $M_{\rm ecl,max}(\psi(t))$ are the minimum and

maximum possible masses of the embedded clusters in a population of clusters, respectively, and $m_{\rm max} = m_{\rm max}(M_{\rm ecl})$. For $M_{\rm ecl,min}$ we take 5 $M_\odot$ (the mass of a Taurus-Auriga aggregate, which is arguably the smallest star-forming "cluster" known). The upper mass of the embedded cluster population depends instead on the SFR and that makes the whole IGIMF dependent on ψ. The correlation between $M_{\rm ecl,max}$ and SFR has been determined observationally (Larsen & Richtler 2000; Weidner et al. 2004) and results from the sampling of clusters from the embedded cluster mass function given the amount of gas mass being turned into stars per unit time (Weidner et al. 2004).

In Fig. 1, we show the IGIMF as a function of the SFR for the three values of β considered in this work, compared to our standard IMF. The IGIMFs are characterized by a nearly uniform decline, which follows approximately a power law, and a sharp cutoff when m gets close to $m_{\rm max}$. Of course, the steepest distribution of embedded cluster (in our case the model with $\beta = 2.35$) produces also the steepest IGIMF because this distribution is biased towards embedded clusters of low mass, therefore the probability of finding high mass stars in this cluster population is lower. Moreover, the dependence of the IGIMF on the SFR is strong for SFR ≤ 1 $M_\odot$ yr^{-1} whereas it is very mild for SFR ≥ 1 $M_\odot$ yr^{-1} (see Recchi et al. 2009). This is due to the fact that for SFRs larger than ~ 1 $M_\odot$ yr^{-1} the maximum possible mass of the embedded cluster is very high, therefore it is always possible to sample massive stars in the whole galaxy up to a mass very close to the empirical limit (which is assumed to be 150 $M_\odot$; see Weidner & Kroupa 2005). All the IGIMFs are normalized in mass to unity as the standard IMF (see eq. 2).

The standard IMF is steeper in the low mass range, i.e. for stellar masses $m \leq 0.5$ $M_\odot$. These masses do not contribute to the chemical enrichment of the Galaxy, since they have lifetimes larger than the Hubble time. However, their distribution remains unchanged during the evolution of the Galaxy and it can be constrained by analysing the present-day mass function (see Sect. 4.8).

3 THE CHEMICAL EVOLUTION MODEL

The adopted chemical evolution model is calibrated in order to reproduce a large set of observational constraints for the Milky Way galaxy (Chiappini et al. 2001). The Galactic disc is approximated by several independent rings, 2 kpc wide, without exchange of matter between them. The Milky Way is assumed to form as a result of two main infall episodes. During the first episode, the halo and the thick disc are formed. During the second episode, a slower infall of external gas forms the thin disc with the gas accumulating faster in the inner than in the outer region ("inside-out" scenario, Matteucci & François 1989). The process of disc formation is much longer than the halo and bulge formation, with time scales varying from ~ 2 Gyr in the inner disc to ~ 7 Gyr in the solar region and up to 20 Gyr in the outermost disc. In this paper, we are interested in the effects of a time-variyng IMF in the Solar Neighbourhood. For this purpose, we focus on a ring located at 8 kpc from the Galactic centre, 2 kpc wide.

For a single-phase gas, the chemical evolution of a given chemical element i is computed through the following equation:

$$\begin{aligned}\frac{dG_i(t)}{dt} &= -\dot{\sigma}_*(t)X_i(t) \\ &+ \int_{M_L}^{M_{B_m}} \dot{\sigma}_*(t-\tau_m)Q_{\rm mi}(t-\tau_m)\xi^{'}(m,t)dm \\ +A_{Ia}\int_{M_{B_m}}^{M_{B_M}} &\int_{\mu_{\rm min}}^{0.5} f(\mu)Q_{\rm mi}(t-\tau_{\rm m_2})\xi^{'}(m,t)\dot{\sigma}_*(t-\tau_{\rm m_2})d\mu dm \\ &+(1-A_{Ia})\int_{\rm M_{B_m}}^{\rm M_{B_M}} \dot{\sigma}_*(t-\tau_m)\,Q_{\rm mi}(t-\tau_m)\xi^{'}(m,t)dm \\ &+\int_{\rm M_{B_M}}^{M_U(t)} \dot{\sigma}_*(t-\tau_m)Q_{\rm mi}(t-\tau_m)\xi^{'}(m,t)dm \;+(\frac{dG_i(t)}{dt})_{\rm inf},\end{aligned} \tag{4}$$

where $G_i(t) = \sigma_g(t)X_i(t)/\sigma_{tot}$ is the gas surface mass density in the form of an element i normalized to a total surface mass density σ_{tot}, and $G(t) = \sigma_g(t)/\sigma_{tot}$ is the total fractional mass of gas present in the galaxy at the time t. $X_i(t)$ is the abundance by mass (or mass fraction) of the element i. The quantity $\dot{\sigma}_*(t)$ is the surface SFR density. In general, this quantity is a function of the galactic radius r:

$$\dot{\sigma}_*(r,t) = \nu[\frac{\sigma(r,t)}{\sigma(r_\odot,t)}]^{2(k-1)}[\frac{\sigma(r,t_{Gal})}{\sigma(r,t)}]^{k-1}\sigma_g^k(r,t) \tag{5}$$

(Chiappini et al. 1997), where ν is the SF efficiency, $\sigma(r,t)$ is the total mass (gas + stars) surface density at a radius r and time t ($t_{Gal} = 14$ Gyr is the present age of the Milky Way), $\sigma(r_\odot,t)$ is the total surface mass density in the solar region and $\sigma_g(r,t)$ is the ISM surface mass density. In this paper, we focus on the solar neighbouhod and we assume $r = r_\odot = 8kpc$. For the gas density exponent k a value of 1.5 has been assumed by Chiappini et al. (1997) in order to ensure a good fit to the observational constraints for a large set of local spirals (Kennicutt 1998). The efficiency of SF is set to $\nu = 1$ Gyr^{-1}, and becomes zero when the gas surface density drops below a certain critical threshold. For the SF, we adopt a threshold gas density $\sigma_{th} \sim 7M_\odot pc^{-2}$ in the disc as suggested by Kennicutt (1989).

The second term in Eq. 4 is the rate at which each element is restored into the ISM by single stars with masses in the range M_L - M_{B_m}, where M_L is the minimum mass contributing, at a given time t, to chemical enrichment (the minimum is $0.8M_\odot$) and M_{B_m} is the minimum mass allowed for binary systems giving rise to type Ia SN ($3M_\odot$, Matteucci & Greggio 1986). The quantity

$$\xi^{'}(m,t) = m\,\xi(m,t) \tag{6}$$

is the initial mass function in mass and in the standard case is given by $\xi^{'}_{std} = m\,\xi_{std}$, described in Sect. 2.1 and is constant in time, otherwise it is a function of the initial stellar mass m and of the time t and is computed with the method described in Sect. 2.2. The quantities $Q_{mi}(t-\tau_m)$ (where τ_m is the lifetime of a star of mass m) contain all the information about stellar nucleosynthesis for elements either produced or destroyed inside stars or both (Talbot and Arnett 1971; Matteucci 2001). The third term represents the enrichment due to binaries which become type Ia SNe, i.e. all the binary systems with total mass between M_{B_m}

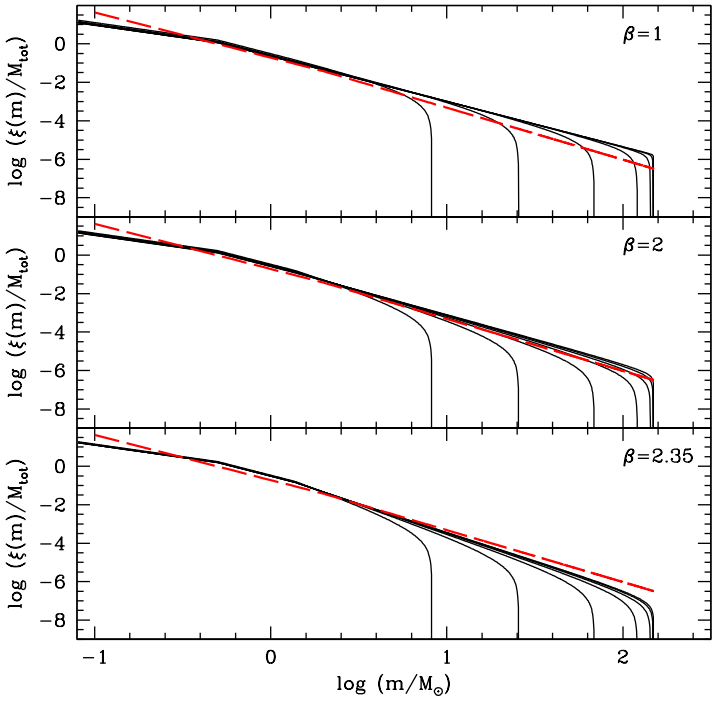

Figure 1. IGIMFs for different cluster mass functions distributions. Upper panel: $\beta = 1$; central panel: $\beta = 2$; lower panel: $\beta = 2.35$. In each panel we have considered 7 possible values of SFRs, ranging from 10^{-4} $M_{\odot}$ yr^{-1} (lowermost solid lines) to 100 $M_{\odot}$ yr^{-1} (uppermost solid lines), equally spaced in logarithm. The thick dashed line is the standard IMF used in this work (see Sect. 2.1). The IGIMFs and the standard IMF are all normalized through the equation $\int m\xi(m)dm = M_{tot} = 1M_{\odot}$.

and $M_{B_M} = 16M_{\odot}$. For the type Ia SN progenitor model, the Single Degenerate (SD) scenario is assumed, where a C-O white dwarf explodes by C-deflagration mechanism after having reached the Chandrasekhar mass ($1.44M_{\odot}$), owing to progressive mass accretion from a non-degenerate companion (Whelan & Iben 1973). This model is still one of the best to reproduce the majority of the properties of local galaxies (Matteucci et al. 2006; Calura & Matteucci 2006; Matteucci et al. 2009). The parameter A_{Ia} represents the unknown fraction of binary systems with the specific characteristics to become type Ia SNe in the range 3-16 $M_{\odot}$ and is fixed by reproducing the observed present time SN Ia rate (Calura & Matteucci 2006). In this third term, both quantities $\dot{\sigma}_*$ and Q_{mi} refer to the time $t - t_{m_2}$, where t_{m_2} indicates the lifetime of the secondary star of the binary system, which regulates the explosion timescale. $\mu = M_2/M_B$ is the ratio between the mass of the secondary component M_2 and the total mass of the binary system M_B, whereas $f(\mu)$ is the distribution function of this ratio. Statistical studies indicate that mass ratios close to 0.5 are preferred, so the formula:

$$f(\mu) = 2^{1+\gamma}(1+\gamma)\mu^{\gamma} \quad (7)$$

is commonly adopted, with $\gamma = 2$ (Matteucci & Recchi 2001). μ_{min} is the minimum mass fraction contributing to the SNIa rate at the time t, and is given by

$$\mu_{min} = max\left\{\frac{M_2(t)}{M_B}, \frac{M_2 - 0.5M_B}{M_B}\right\}. \quad (8)$$

The fourth term represents the enrichment due to stars in the mass range M_{B_m} - M_{B_M} which are either single, or, if in binaries, do not produce a SN Ia event. In this mass range, all the stars with masses $m > 8M_{\odot}$ will explode as type II SNe, which in our picture are assumed to originate from core collapse of single massive stars. The fifth term of Eq. 4 represents the enrichment of stars more massive than M_{B_M}, all of which explode as core collapse (i.e mostly type II, see Calura & matteucci 2006) SNe. The upper mass limit contributing to chemical enrichment is $M_{U(t)}$ and is a function of time through the IMF, $\xi^{'}(m,t)$. We assume that the maximum value for $M_{U(t)}$ is 100 $M_{\odot}$. The assumption of a maximum stellar mass 150 $M_{\odot}$ would have a negligible effect on the results presented in this paper. Finally, the last term accounts for the infall of external gas.

It is worth stressing that equation 4 differs substantially from the classic formalism used in most of the previous chemical evolution models (e.g. Matteucci & Greggio 1986; Chiappini et al. 2001), which use an IMF constant in time, whereas in this case the IMF is a function of the SFR, which is a function of cosmic time. Later on, we will see how the time variations of the IGIMF depend on the star formation history for various values of the parameter β.

The rate at which the thin disc is formed out of external matter is

$$(\frac{dG_i(t)}{dt})_{\rm inf} = B(R)\, e^{-(t-t_{max})/\tau_D}, \quad (9)$$

where t_{max} is the time of maximum gas accretion onto the disc, corresponding to the end of the halo-thick disc phase

and it is equal to 1 Gyr. The quantity τ_D is the timescale for mass accretion onto the thin disc component. Following Romano et al. (2000) and Chiappini et al. (2001), we assume that τ_D increases with increasing Galactic radius

$$\tau_D(R) = 1.033 \times R - 1.267. \quad (10)$$

The constant $B(R_\odot)$ is fixed in order to reprodue the present-day total surface mass density (stars + gas) in the solar neighbourhood. Concerning the nucleosynthesis prescriptions, we assume the yields of Van den Hoeck & Groenewegen (1997) for low and intermediate mass stars, the yields of Iwamoto et al. (1999) for type Ia SNe and those of François et al. (2004) for massive stars. In Table 1, we show the standard assumptions for the main parameters of our chemical evolution model.

3.1 Observational data set

In Table 2, we show the solar neighbourhood observables used in this paper, with their values and references.
Concerning the observed type Ia and type II SN rates, as observational data we use the values of Capellaro (1996), expressed in $century^{-1}$ and valid for the whole MW disc. To compare them with the predictions, we divide the observed values by the area of the MW disc, which, assuming a radius of $\sim$ 15 kpc, is roughly $S_{disc} \sim 10^9 pc^2$. In this way, for the type Ia and type II SN rates we obtain values of 0.003 $pc^{-2}\mathrm{Gyr}^{-1}$ and 0.012 $pc^{-2}\mathrm{Gyr}^{-1}$, respectively.

Concerning the stellar surface density of visible stars and remnants, as observational value we use an indirect estimate. In a recent paper, Weber & de Boer (2009) discuss the uncertainty of the total local visible surface density. They provide a value of $48 \pm 9\ M_\odot/pc^2$. This value is in agreement with another recent estimate of Holmberg & Flynn (2004), which found 53 $M_\odot/pc^2$ in visible matter, and is consistent with the value we achieve with our standard model, 50 $M_\odot/pc^2$.

The local gas surface density is between 7 and 14 $M_\odot/pc^2$ (Kulkarni & Heyles 1987, Dame 1993, Olling & Merrifield 2001). A reasonable value based on this data is $10.5 \pm 3.5\ M_\odot/pc^2$. This value is also consistent with our estimate from the standard model. By combining these two quantities, i.e. by subtracting the gas density from the total density and by combining the errors, for the local mass density in stars and remnants we obtain $37.5 \pm 10 M_\odot/pc^2$. This estimate is compatible with previous values based on the combination of the observed stellar mass density and the one in stellar remnants (Gilmore et al. 1989, Mera et al. 1998).

3.2 IGIMF and Star Formation Rate

In Section 2, we have seen that the IGIMF is a function of the total SFR $\psi(t)$, expressed in $M_\odot/yr$. In particular, the upper mass limit of the IGIMF is sensitive to the value of the star formation rate.
Our chemical evolution code is designed to produce all physical quantities as surface mass densities, so the direct output of our code is a SFR surface density (the quantity $\dot{\sigma}_*$ defined in Sect. 3). To convert the SFR density into the appropriate units, we perform the following assumptions. The solar neighbourhood is described by a 2 kpc-wide ring located at the galactocentric distance of 8 kpc from the centre. The area of this ring is $S_\odot \sim 10^8$ pc^2. The SFR $\psi(t)$ can be calculated from the SFR surface density $\dot{\sigma}_*$ as

$$\psi(t) = \dot{\sigma}_* \cdot S_\odot \cdot 10^{-9}. \quad (11)$$

In this way, we obtain for our standard model a present value of $0.26 M_\odot/yr$. If we consider that the local observed SFR density is $3.5 M_\odot pc^{-2} yr^{-1}$ and we convert this value into the same units, we obtain $0.35 M_\odot/yr$, consistent with the above estimate.

4 RESULTS

Our aim is to test the effects of the IGIMF on the chemical evolution of the S.N., taking into account a large set of available observational constraints. First, we will consider the effects of the SFR-dependent IGIMF on the predicted physical properties of the solar neighbourhood. Then, we will discuss all of the observables and the main parameters which can be tested by our analysis. Finally, we will see how a fine-tuning of the parameters considered in this work may allow us to derive constraints on the local IMF.

4.1 The fitness test

In order to quantitatively compare our results with the observables considered in this paper, we adopt the formula

$$fitness = \frac{1}{1+\delta} \quad ; \quad \delta = \Sigma_i \frac{w(i)[\mathrm{obs}(i) - \mathrm{theo}(i)]^2}{\max\left\{[\mathrm{obs}(i)]^2, [\mathrm{theo}(i)]^2\right\}} \quad (12)$$

where, for the i-th value of each considered parameter, obs (i) and theo (i) are the observed values and the predictions of the model, respectively (see also Růžička et al. 2007; Theis & Kohle 2001). We have also introduced a weight $w(i)$ for each observable i in order to give each set of observables the same statistical weight. To be more precise: we have grouped the observables in 5 groups: (1) physical quantities (SFR, SNR_{II}, SNR_{Ia}, Σ_*, Σ_{gas}); (2) solar abundances; (3) average [α/Fe] ([O/Fe], [Si/Fe]) ratios for each bin of [Fe/H]; (4) dN/d[Fe/H] (SMD) in each bin of [Fe/H]; (5) present-day mass function in each bin of mass. We have chosen a weight such that $w(i)$ multiplied by the members of each group gives always the same number. This means that in the fitness calculation, the same weight is given to all the 5 groups of observables. Following this approach, each single observable in the physical quantities group has the largest weight, and this occurs because the physical quanties group is the one having the smallest number of members (5). On the other hand, each single member of the [α/Fe] group, counting the highest member number (28), has the lowest one, but, as already stressed, the [α/Fe] group as a whole has the same weight of the physical quantities group. Of course, the closer $fitness$ is to 1, the better the model is in reproducing the observations. In Fig. 4, we show the "fitness" quantity as a function of β for all the models considered in this paper. The results obtained for each value of β will be discussed separately.

Table 1. Parameters for the standard model of the solar neighbourhood.

Parameter	Adopted value
SF efficiency ν (Gyr^{-1})	1
Infall timescale for the thin disc τ_D (Gyr)	7
Gas density threshold for SF ($M_\odot/pc^2$)	7
Fraction A_{Ia} of binary systems originating type Ia SNe	0.04

Table 2. Solar neighbourhood observables used in this paper and references.

Observable	value	Reference
SFR Surface density	$3.5 \pm 1.5\ M_\odot\, pc^{-2}\, Gyr^{-1}$	Rana (1991)
type Ia SNR	$0.003 \pm 0.002\ pc^{-2}\, Gyr^{-1}$	Cappellaro (1996)
type II SNR	$0.012 \pm 0.008\ pc^{-2}\, Gyr^{-1}$	Cappellaro (1996)
Gas surface density	$10.5 \pm 3.5\ M_\odot\, pc^{-2}$	Kulkarni & Heiles (1987) Dame (1993) Olling & Merrifield (2001)
Stellar surface density (visible stars and remnants)	$37.5 \pm 10\ M_\odot\, pc^{-2}$	Weber & de Boer (2009)
Stellar abundance ratios	-	various authors
Stellar Metallicity distribution	-	various authors
Present-day mass function	-	various authors

4.2 The effects of the IGIMF on the properties of the solar neighbourhood

In Fig. 2 we show the effects of the standard IMF and of the IGIMF assuming three different values for β on the calculated evolution of the star formation rate, of the type Ia and II SN rates and of the stellar and gas mass surface density.

All the models shown in Fig. 2 are characherised by the same value for the star formation efficiency, $\nu = 1$ Gyr^{-1}. In this way, it is possible to appreciate the effects of varying the IMF, keeping all the other parameters constant.

The most striking features of the standard model are the SF hiatus at 1 Gyr (see Chiappini et al. 1997, 2001) and the threshold-dominated SF after 10 Gyr.

The hiatus in the SF is due to the transition between the end of the halo/thick-disc phase and the beginning of the thin-disc phase. This effect is confirmed by the relation between [Fe/O] and [O/H] observed in local stars (Chiappini et al. 1997; Gratton et al. 2000) and can be naturally reproduced once a SF threshold is adopted (Chiappini et al. 2001).

Moreover, in the standard model the adoption of a SF threshold causes numerous oscillations in the calculated SFH, which is also reflected in the SNRs.

Within the first 2 Gyr of evolution, the SFRs of the standard model and the ones calculated for the models adopting the IGIMF are all very similar. The SF hiatus is visible also in the models with the IGIMF, and this indicates that the threshold effect is important in all the four cases studied in Fig. 2. For times larger than 2 Gyr, the SFRs for models computed with the IGIMF are not very sensitive to the adoption of the SF threshold, with the exception of the model with $\beta = 2.35$, which experiences some threshold-induced star-formation gasping at times > 12 Gyr. The reason why the models with $\beta = 1$ and $\beta = 2$ are not influenced by the threshold is that in these two cases the IGIMF is flatter than the standard IMF (Fig. 1), which implies larger mass ejection rates and consequently larger gas masses available for star formation. The type Ia and type II SN rates computed with $\beta = 1$ and $\beta = 2$ are higher than those computed with the standard IMF because the SFR values are slightly larger at any time. On the other hand, in the case with $\beta = 2.35$ the SN rates are lower than in the standard case because the IGIMF is slightly steeper than the standard IMF in the mass range of the type Ia and type II SN progenitors.

The evolution of the gas surface mass density is weakly sensitive to the adopted value of β. As explained above, a lower β implies a higher mass ejection rate from dying stars, consequently a larger gas mass at any time. The fact that the stellar mass surface density computed with the standard IMF flattens at times > 10 Gyr is basically due to the

effect of the star formation threshold, which inhibits star formation at late evolutionary times. This flattening is not predicted for the three cases computed adopting the IGIMF since, as we have already seen, the star formation histories are not strongly influenced by the SF threshold.

In Fig. 3, we show the predicted time evolution of the [Fe/H] (lower panel) and the [O/Fe] - [Fe/H] plot. In general, lower values of β, corresponding to flatter IGIMFs, produce at any time higher [Fe/H] values and higher [α/Fe] values at a given metallicity.

4.3 Local observables and their dependence on model parameters

The observables considered in this paper, summarized in Tab. 2, are:

- the abundance ratios, observed in local stars of various metallicities; The abundance ratios between two elements formed on different timescales are very useful diagnostics, since they allow us to constrain the star formation history of the studied system. They provide us with information on the relative roles of various stellar sources in the chemical enrichment of the interstellar medium (Matteucci 2001). In particular, the study of [α/Fe][‡] is of major importance, owing to the difference in the timescales for α-elements and Fe production. The abundance ratios are sensitive to the assumption of the IMF and to the star formation history.

- the solar abundances, which are useful to test whether our models correctly reproduce the metallicity of the Sun at the epoch when the Solar System formed, i.e. ~ 4.5 Gyr ago; The solar abundances provide information on the integrated star formation history.
- the observed stellar metallicity distribution, which tells us the differential distribution of the living stars as a function of [Fe/H];
- the present-day type Ia and type II SN rates, which are sensitive to the star formation history, to the stellar IMF and to the fraction of binary systems able to produce type Ia SNe;
- the present-day gas surface mass density, sensitive mostly to the star formation history
- the present-day stellar surface density, depending mainly on the star formation history
- the present-day mass function, depending on the combination of the initial mass function and the star formation history.

In the following, we will present all our results obtained with the IGIMF assuming three different values for the index β of the star cluster mass function. The results obtained with the IGIMF are compared to those obtained by means of the standard IMF. In each case, we aim at obtaining the best match between our models and the set of observational constraints by varying the star formation efficiency ν . In every single case for β, the best model is the one providing the best match simultaneously to the calculated SN rates, gas and stars mass surface densities, solar abundances, abundance ratios and present-day mass function.

We do not consider the infall timescale as a free parameter. Our assumption is based on the fact that numerical dynamical models for disc galaxy formation indicate infall time-scales of several Gyr (Larson 1976; Samland et al. 1997). An infall timescale of 5-6 Gyr is indicated also by cosmological SPH simulations of disc galaxies in a standard Λ-cold dark matter cosmology (Sommer-Larsen et al. 2004). However, we have tested the effects of varying the infall timescale, verifying that variations of the e-folding time τ of 1-2 Gyr have a negligible impact on our results.

4.4 $\beta = 1$

In Fig. 5, we show the star formation history, the time evolution of the type Ia and type II SN rates, of the gas surface density and of the stellar mass density for three models with $\beta = 1$ and assuming various SF efficiencies ν, compared to the results obtained with the standard IMF. By assuming $\beta = 1$ for the embedded cluster mass function, the model which best reproduces our set of observational constraints is characterized by a SF efficiency $\nu = 0.1$ Gyr^{-1}. This can be seen from Fig. 4, where we show how the "fitness" quantity defined in section 4 behaves as a function of β. Among the models with $\beta = 1$, the one with the highest fitness value is that with $\nu = 0.1$ Gyr^{-1}.

From Fig. 5 it is clear that there are some observables which cannot be reproduced accurately, such as the present gas and stellar mass densities. Furthermore, All the models with $\beta = 1$ tend to overestimate the type II SN rate. This result should be expected, since the assumption $\beta = 1$ produces an IMF flatter than the standard one, hence richer in massive stars.

In Table 3, we present the predicted solar abundances for the most important heavy elements, obtained with the standard IMF and with the best models using the IGIMFs for various β. We limit our calculations to the cases of the most important chemical elements, for which the standard model reproduces the observed abundance pattern with the most accurate precision.

In the case $\beta = 1$, the IGIMF being flatter than the standard IMF implies heavy element abundances higher than the solar ones. By decreasing further the SF efficiency, it is possible to improve the match between the observed solar abundances and the predicted ones, but at the expense of the match of the local gas and star surface mass densities.

In Fig. 6, we present the abundance ratios as a function of metallicity, traced by $[Fe/H]$, computed by means of our standard chemical evolution model and compared to three models with $\beta = 1$ and different SF efficiencies. As expected, owing to the excess of massive stars and to the very high type II SN rates, the predictions obtained with the IGIMF and $\beta = 1$ overestimate all the [α/Fe] ratios. It is also interesting to note that the results are weakly dependent on the SF efficiencies for values in the range $0.1 \leq \nu/\mathrm{Gyr}^{-1} \leq 0.5$.
In Fig. 7, we show instead the stellar metallicity distribution computed by means of our standard IMF and with the IGIMF, showing results for three different SF efficiencies. The standard IMF allows us to reproduce the observed stel-

‡ All the abundances between two different elements X and Y are expressed as $[X/Y] = log(X/Y) - log(X/Y)_{\odot}$, where (X/Y) and $(X/Y)_{\odot}$ are the ratios between the mass fractions of X and Y in the ISM and in the Sun, respectively. We use the set of solar abundances as determined by Grevesse at al. (2007).

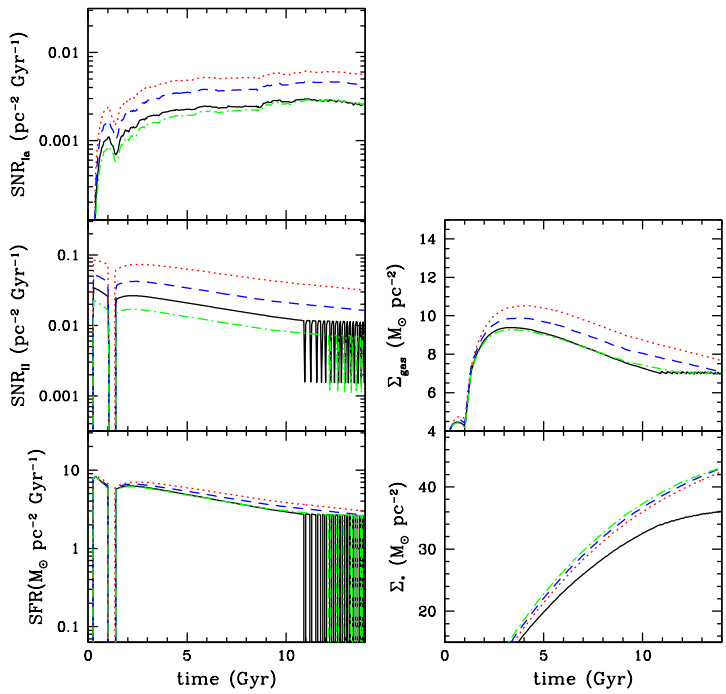

Figure 2. From top-left, anti-clockwise: time evolution of the type Ia SNR, type II SN rate, SFR, surface density in stars and in gas computed with the standard IMF (solid lines) and with the IGIMF assuming $\beta = 1$ (dotted lines), $\beta = 2$ (dashed lines) and $\beta = 2.35$ (dot-dashed lines). For all the models we have assumed the same value for the star formation efficiency, $\nu = 1\,\mathrm{Gyr}^{-1}$.

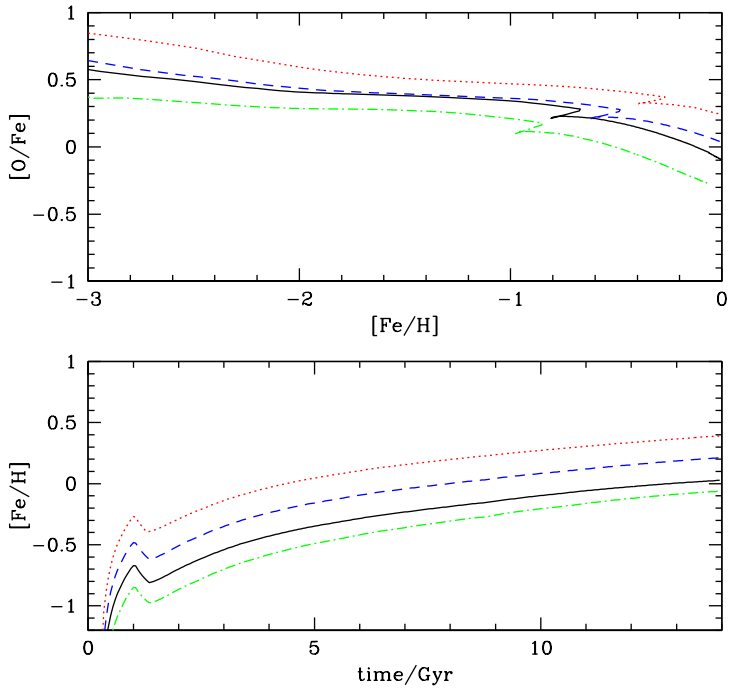

Figure 3. Time evolution of the interstellar [Fe/H] (lower panel) and [O/Fe]-[Fe/H] relation (upper panel) computed with the standard IMF (solid lines) and with the IGIMF assuming $\beta = 1$ (dotted lines), $\beta = 2$ (dashed lines) and $\beta = 2.35$ (dot-dashed lines). For all the models we have assumed the same value for the star formation efficiency, $\nu = 1\,\mathrm{Gyr}^{-1}$.

Table 3. Fractional mass in the Sun for various elements as observed by Grevesse et al. (2007, second column) and as predicted by means of our model by assuming the standard IMF (third column) and for our best models adopting the IGIMF computed with $\beta = 1$ (fourth column), $\beta = 2$ (fifth column), and $\beta = 2.35$ (sixth column).

Element	Obs. (G07)	standard IMF	IGIMF $\beta = 1$	IGIMF $\beta = 2$	IGIMF $\beta = 2.35$
H	0.7395	0.735	0.732	0.721	0.730
He	0.2485	0.253	0.251	0.260	0.259
C	2.18(-3)	1.83(-3)	1.72(-3)	2.57(-3)	2.47(-3)
O	5.41(-3)	5.5(-3)	8.819(-3)	8.20(-3)	3.35(-3)
Mg	6.01(-4)	7.0(-4)	8.89(-4)	1.10(-3)	4.94(-4)
Si	6.70(-4)	7.6(-4)	9.19(-4)	1.20(-3)	6.35(-4)
Fe	1.17(-3)	1.21(-3)	1.19(-3)	1.96(-3)	1.32(-3)
Z	0.012	0.0126	0.016	0.019	0.010

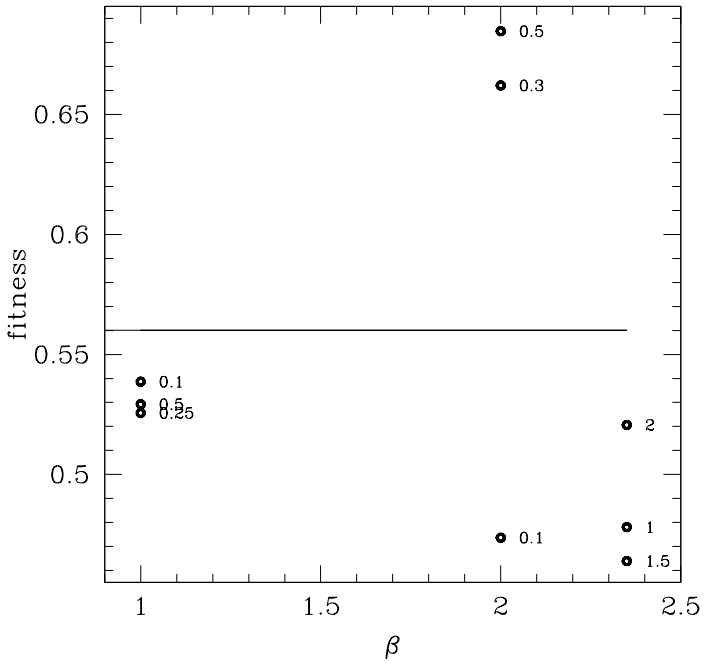

Figure 4. Open circles: fitness (defined in Section 4) as a function of β for various models, each one characterized by a particular star formation efficiency ν, indicated by the number beside each open circle. The horizontal line indicates the fitness value computed for the standard model. From this figure it is clear that the model with $\beta = 2$ and $\nu = 0.5$ is the one providing the best fit to the set of observables studied in this paper.

lar metallicity distribution (SMD) with good accuracy, concernig either the low-metallicity tail and the peak metallicity value. In Fig. 7, we show both the weighted and reconstructed SMDs as observed by Jorgensen (2000). The error bars are provided only for the reconstructed SMD and are also plotted in Fig. 7. By means of our best model computed with the IGIMF and $\beta = 1$, the predicted SMD is not well reproduced. The peak metallicity is underestimated, and the number of stars with metallicity in the range -0.5≤[Fe/H]< −0.25 is overestimated. On the other hand, the high-metallicty tail is remarkably in disagreement with the observations. Models characterised by higher star formation efficiencies lead to an overabundance of stars with metallicity [Fe/H]>0 with respect to the observations.
We can conclude that, by assuming $\beta = 1$, no model can satisfactorily reproduce at the same time all the observables considered in this work.

4.5 $\beta = 2$

In Fig. 8, we present the star formation history, the time evolution of the type Ia and type II SN rates, of the gas sur-

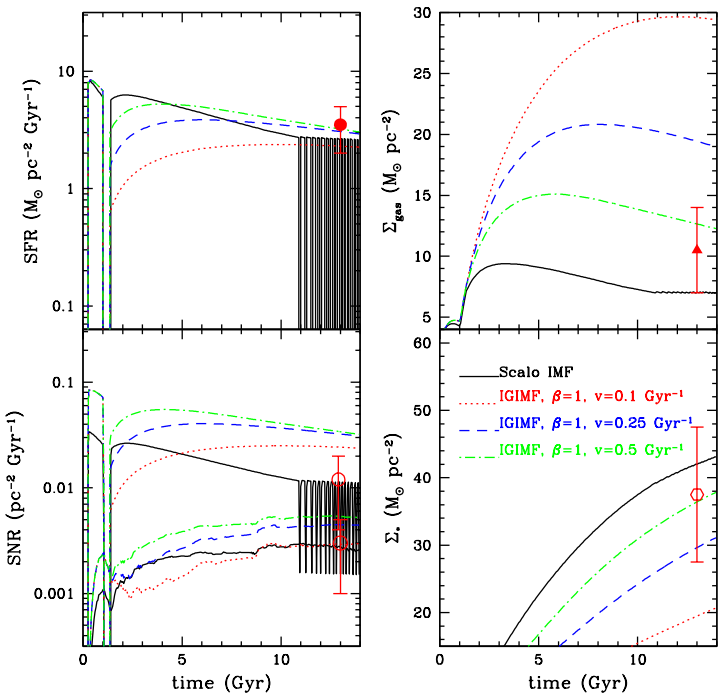

Figure 5. From top-left, clockwise: calculated time evolution of the star formation history, of the gas surface density, stellar surface density and SN rates computed by means of the solar neighbourhood model with the standard IMF (solid lines) and by means of three models with the IGIMF, in the case $\beta = 1$ and assuming three different SF efficiencies: $\nu = 0.1$ Gyr^{-1} (dotted lines), $\nu = 0.25$ Gyr^{-1} (dashed lines), and $\nu = 0.5$ Gyr^{-1} (dash-dotted lines). In the panel showing the SN rate evolution, the lower and upper curves represent the calculated type Ia and type II SN rates, respectively. Observational data are reported in Tab. 2.

face density and of the stellar mass density for three models with $\beta = 2$ and different SF efficiencies ν, compared to the results with the standard IMF and to the available local observations. The case with $\beta = 2$ is more promising than the previous one for reproducing the constraints considered in this work. In this case, the model which best reproduces our set of observational constraints is characterized by a SF efficiency $\nu = 0.5$ Gyr^{-1} (see Fig. 4), althogh also the model with SF efficiency $\nu = 0.3$ Gyr^{-1} provides satisfactory results, as shown by the fitness test. We have also tested models with SF efficiency $\nu > 0.5$ Gyr^{-1}, finding fitness values lower than the one found with $\nu = 0.3 - 0.5$ Gyr^{-1}.

Both type Ia and II SNRs are larger than those predicted with the standard IMF. However, both the present-day SN rates predicted with the IGIMF are consistent with the local observations by Cappellaro (1996). The gas and stellar surface densities predicted with the best model with the IGIMF are in agreement with the observed values.

In the fourth column of Table 3, we present the solar abundances predicted with the best model with the IGIMF and $\beta = 2$. As can be seen from Fig. 8 and Table 3, a satisfactory match between the predictions and the observations is achievable in this case, although the heavy element abundances are slightly overestimated.

In Fig.9 we show the abundance ratios as a function of [Fe/H], compared to available observations in local stars. In this case, the main trends of the observed abundance ratios as a function of [Fe/H] are well accounted for, as well as the abundance ratios at the solar [Fe/H].

The results obtained with this choice of β are quite similar to the ones achieved with the standard IMF. This result could be expected since, as shown in Fig. 1, in the intermediate case with $\beta = 2$ the IGIMF is very similar to the standard IMF. However, the IGIMF is slightly more top-heavy than the standard IMF. For the best model, this translates into $[\alpha/Fe]$ ratios sligthly larger than those computed with the standad IMF.

As shown in Fig. 10, it is possible to obtain good results also for the SMD, with very little difference between the model characterized by $\nu = 0.3$ Gyr^{-1} and $\beta = 2$ and the standard model. On the other hand, the model with the IGIMF $\nu = 0.5$ Gyr^{-1} is slightly overestimating the number of high metalicity stars. However, globally, with $\beta = 2$ satisfactory results can be achieved also concerning the study of the stellar metallicity distribution.

We can conclude that the assumption of $\beta = 2$ allows us to satisfactorily reproduce the set of observational constraints considered in this work. This is an important result, given the fact that the IGIMF is computed from first principles. Furthermore, this result allows us to constrain the embedded cluster mass function. In the case this function may be approximated by a power law, here we have shown that the index $\beta = 2$ is to be favoured with respect to the case $\beta = 1$.

The results with $\beta = 2$ are very similar to those obtained with the standard IMF, and in principle, on the basis of the results described in this section, it may be difficut to

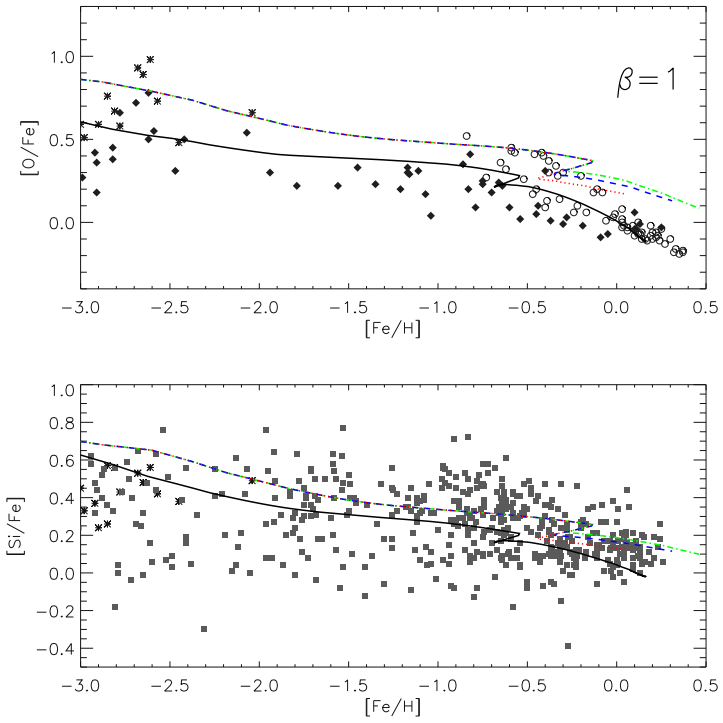

Figure 6. Predicted [O/Fe]-[Fe/H] (upper panel) and [Si/Fe]-[Fe/H] (lower panel) computed by means of the solar neighbourhood model with the standard IMF (solid lines) and by means of three models with the IGIMF, in the case $\beta = 1$ and assuming three different SF efficiencies: $\nu = 0.1$ Gyr^{-1} (dotted lines), $\nu = 0.25$ Gyr^{-1} (dashed lines), and $\nu = 0.5$ Gyr^{-1} (dash-dotted lines). The predictions are compared to observational data from various authors. Asterisks: Cayrel et al. (2004); open circles: Bensby et al. (2003); solid diamonds: François et al. (2004). The solid squares are from a compilation of data by Cescutti (2008).

discriminate between the two scenarios. In Sect. 4.8, we will suggest the use of a diagnostic allowing us to put further constraints on the IMF in the solar neighbourhood and to disentangle between the standard IMF and the IGIMF.

4.6 $\beta = 2.35$

The assumption of $\beta = 2.35$ produces fewer massive stars than in the standard case, and this has some impact on the predicted SN rates and gas and stellar surface mass densities. In Fig.s 11, 12, and 13 we show the predicted time evolution of the SFR, SN rates, gas and stellar mass densities computed by assuming the IGIMF with $\beta = 2.35$ and SF efficiencies $\nu = 1$ Gyr^{-1}, $\nu = 1.5$ Gyr^{-1}, and $\nu = 2$ Gyr^{-1}, respectively, compared to the standard model and to the local observational values. In the sixth column of Table 3 we show the solar abundances predicted with the best model with $\beta = 2.35$, characterized by a SF efficiency $\nu = 2$ Gyr^{-1} (see Fig. 4). This implies a quicker gas consumption timescale and stronger effects of the SF threshold than in the standard case, which has a SF efficiency $\nu = 1$ Gyr^{-1}. While the model with the standard IMF is influenced by the SF threshold only at times > 11 Gyr, the adoption of a higher SF efficiency causes strong threshold effects already after 1 Gyr of evolution. This is visible mainly in the predicted SF history, type II SNR and gas surface density evolution.

For some elemnents (O,Mg), the model reproducing best the data of Fig. 11 provides solar abundances lower than the observed ones (see Tab. 3). On the other hand, as shown by Fig. 14, the analysis of the abundance ratios as a function of metallicity indicates [α/Fe] values lower than the ones computed with the standard IMF. Finally, in Fig. 15, we show the SMD computed with the IGIMF assuming $\beta = 2.35$ compared to the observations and the results of the standard IMF. In this case, the peak metallicity computed with the IGIMF is shifted leftwards by 0.2 dex with respect to the observations and to the standard model. From the results discussed in this section we can conclude that by assuming $\beta = 2.35$ it is not possible to reproduce at the same time all the observational constraints considered in this paper.

4.7 Effects of other parameters: the star formation threshold and A_{Ia}

At this stage, it may be interesting to study the effects which other important parameters have on our results, such as the SF threshold and the type Ia SN realization probability A_{Ia}.

As shown in Sect. 4.5, the models which best reproduce the constraints considered in this paper are not sensitive to the adopted SF threshold. This is visible from the smooth behaviour of the calculated SF history, whereas we have seen that when the effect of the threshold is important, it presents an oscillatory behaviour, as happens for the SFH of the model with the standard IMF. The case with $\beta = 1$ is characterized by a high amount of mass restored by massive stars into the ISM, keeping its density always significantly above the threshold. Furthermore, in this case the SF effi-

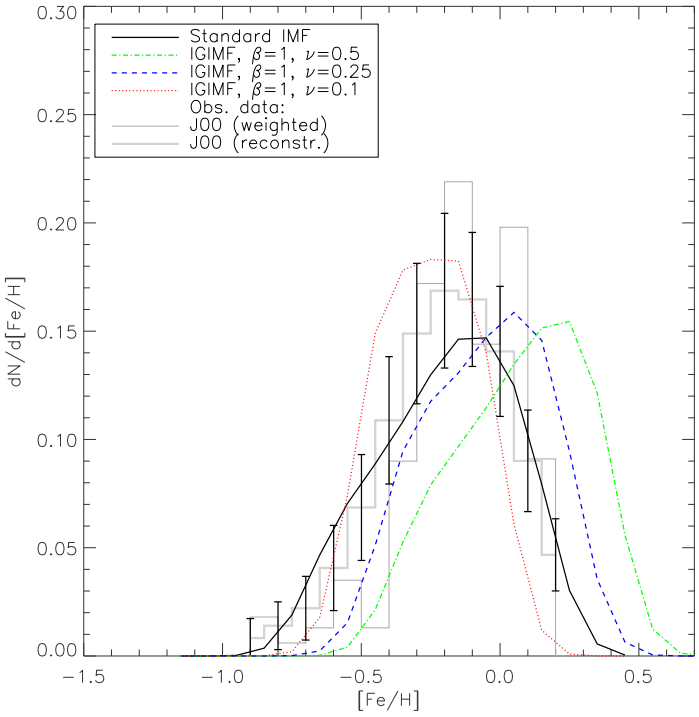

Figure 7. Present-day stellar metallicity distribution in the Solar Neighbourhood. The solid line, the dotted line, the dashed line and the dash-dotted line represent the predicted stellar metallicity distribution computed with the standard IMF and with the IGIMF in the case $\beta = 1$ and SF efficiency $\nu = 0.1$ Gyr^{-1}, $\nu = 0.25$ Gyr^{-1}, and $\nu = 0.5$ Gyr^{-1}, respectively. The thin and thick solid histograms represent the observational weighted and reconstructed SMD from Jorgensen (2000), respectively. For the reconstructed distribution, error bars are plotted.

ciency which allows us to best reproduce the local features is lower than in the standard case. This causes the gas mass to be less efficiently consumed, so that the gas density level is always considerably above the threshold. The same is true for the case with $\beta = 2$. In these two cases, halving the SF threshold to $4M_{\odot}/pc^2$ does not produce any effect on our results. On the other hand, the adoption of a significantly higher threshold, say $> 10M_{\odot}/pc^2$ would be at variance with the observations in local spiral discs (Martin & Kennicutt 2001). The case with $\beta = 2.35$ is the most sensitive to the assumption of the threshold. We show the effects of a threshold $4M_{\odot}/pc^2$ on the star formation history in Fig. 16. The decrease of the threshold causes the SF history to be smoother and to enhance gas consumption, therefore at the present time the galaxy model with $\Sigma_{thr} = 4M_{\odot}/pc^2$ presents a gas density and a stellar density slightly lower and higher than the model with $\Sigma_{thr} = 7M_{\odot}/pc^2$, respectively. On the other hand, the assumption of a lower threshold has no effect on the abundance ratios, and this can be seen in Fig. 17.

It is worth noting that recent GALEX results indicate that the SF cutoff visible from the $H\alpha$ profiles of local star forming galaxies is instead absent in UV profiles (Boissier et al. 2007), suggesting that the existence of a SF threshold may be an observational selection effect, naturally explained by the IGIMF theory as shown by Pflamm-Altenburg & Kroupa (2008). However, as shown by chemical evolution results, the SF threshold is fundamental in reproducing the metallicity gradients observed in the MW and in local galaxies (Chiappini et al. 2001; 2003), unless a variable star formation efficiency through the disc is assumed (Colavitti et al. 2009).

It may be also interesting to discuss the possible effects of the type Ia SN realization probability A_{Ia} on our results. A change in A_{Ia} has effects on the predicted type Ia SN rate, on the [X/Fe]-[Fe/H] plots and on the SMD plot, whereas it leaves unchanged any other quantity studied here. In the case $\beta = 1$, the model which best reproduces our set of observational constraints is characterized by a SF efficiency $\nu = 0.1$ Gyr^{-1}. To reproduce the abundance ratios as a function of [Fe/H], a higher value of A_{Ia} would be required, so that all the curves would move downwards. This would improve also the fit to the observed stellar metallicity distribution, since an increase of the type Ia SN rate efficiciency would shift the computed SMD rightwards, probably in better agreement with the observations. However, as shown in Fig. 5, even with a higher value for A_{Ia}, the observed local type II SN rate, the stellar mass density and the gas density (which do not depend on A_{Ia}) would still not be reproduced. We have seen that in the case $\beta = 2$, no substantial modification of A_{Ia} is required.
Finally, in the case $\beta = 2.35$, a lower value of A_{Ia} would be required to improve our match to the observations in the [X/Fe]-[Fe/H] plot, however this would shift the predicted SMD leftwards, exacerbating the discrepancy between the computed SMDs and the the observed distribution.

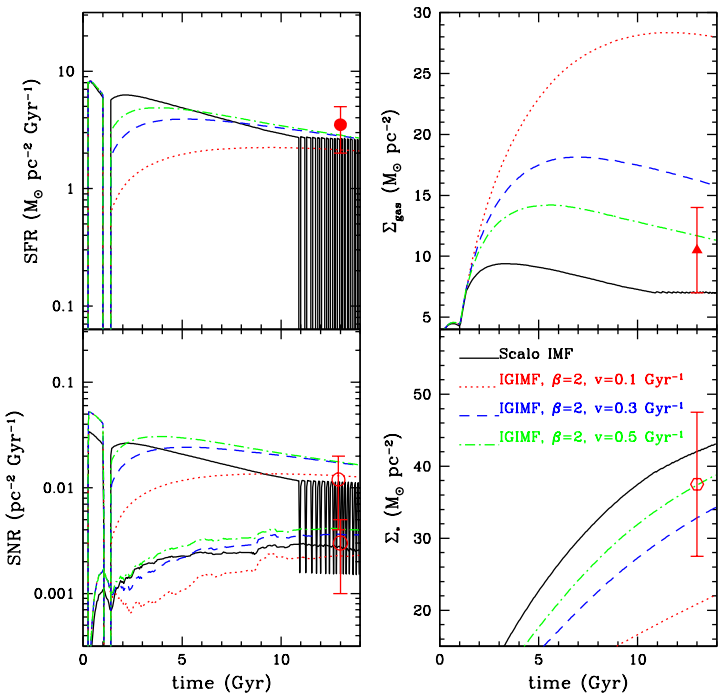

Figure 8. From top-left, clockwise: predicted time evolution of the star formation history, of the gas surface density, stellar surface density and SN rates computed by means of the solar neighbourhhod model with the standard IMF (solid lines) and by means of three models with the IGIMF, in the case $\beta = 2$ and assuming three different SF efficiencies: $\nu = 0.1$ Gyr^{-1} (dotted lines), $\nu = 0.3$ Gyr^{-1} (dashed lines), and $\nu = 0.5$ Gyr^{-1} (dash-dotted lines). Symbols as in Fig. 5.

4.8 The Present-day Mass Function

The present-day mass function (hereinafter PDMF) represents the mass function of living stars as observed in the solar neighbourhood. This quantity is an important diagnostic since it allows us to test, beside the IMF, the star formation history of our best model, providing further information on our parameters complementary to the ones previously discussed.

The number of stars formed in the time interval $(t, t+dt)$ and in the mass interval $(m, m+dm)$ is

$$\xi(m,t)\psi(t)dmdt, \tag{13}$$

(Tinsley 1980). The present number per unit mass of stars with lifetime $\tau_m < T_0$ is

$$n(m) = \int_{T_0-\tau(m)}^{T_0} \psi(t)\xi(m,t)\,dt. \tag{14}$$

The total number of stars with mass between $M_{min} = 0.1M_\odot$ and m is $N(m)$, calculated as

$$N(m) = \int_{M_{min}}^{m} \int_{T_0-\tau(m')}^{T_0} \psi(t)\xi(m',t)\,dt\,dm', \tag{15}$$

where T_0 is the present time, equal to 14 Gyr. The present-day mass function can be calculated as

$$PDMF = dN(m)/d(\log m). \tag{16}$$

In Fig. 18, we show the local PDMF as estimated observationally by various authors, and as predicted by means of our models assuming the standard IMF and the IGIMF for all the three different cases for β, assuming the SF efficiencies of the best models as indicated by our fitness test described in Sect. 4.1. The analytical PDMF of Chabrier (2003) has a log-normal profile for masses $m \leq 1M_\odot$:

$$\frac{d\,N}{d\,(\log m)} \propto exp\{-\frac{(\log\, m\, -\, \log\, m_c)^2}{2\,\sigma^2}\}, \tag{17}$$

with $m_c = 0.079M_\odot$ and $\sigma = 0.69$, and for masses $m > 1M_\odot$ it is given by a power-law:

$$\frac{d\,N}{d\,(\log m)} \propto \begin{cases} m^{-4.37} & \text{if } 0 \leq log(m/M_\odot) \leq 0.54, \\ m^{-3.53} & \text{if } 0.54 \leq log(m/M_\odot) \leq 1.26, \\ m^{-2.11} & \text{if } 1.26 \leq log(m/M_\odot) \leq 1.80. \end{cases}$$

The analytical PDMF of Kroupa et al. (1993) is a power-law:

$$\frac{d\,N}{d\,(\log m)} \propto \begin{cases} m^{-1.3} & \text{if } log(m/M_\odot) \leq -0.3, \\ m^{-2.2} & \text{if } -0.3 \leq log(m/M_\odot) \leq 0, \\ m^{-4.5} & \text{if } 0 < log(m/M_\odot), \end{cases}$$

The Kroupa et al. (1993) and Chabrier (2003) PDMF are very similar at masses $M < 1M_\odot$, and in the same mass range they are in very good agreement with the Miller & Scalo (1979) PDMF. For masses $M > 1M_\odot$, no recent update exists and the reference measures are those of Miller & Scalo (1979) and Scalo (1986), which are in very good agreement in this mass range. In the light of this, for purposes of clarity and to avoid confusion, as observational data in Fig. 18 we plot only the PDMF as determined by Miller & Scalo (1979). This is also the one used for the fitness test described in Sect. 4.1.

From the analysis of Fig. 18, interesting information

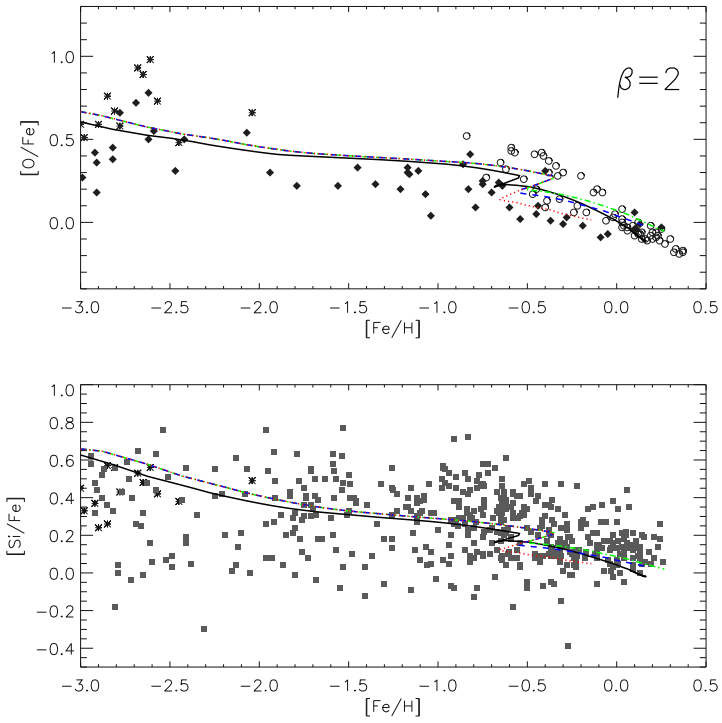

Figure 9. Predicted [O/Fe]-[Fe/H] (upper panel) and [Si/Fe]-[Fe/H] (lower panel) computed by means of the solar neighbourhood model with the standard IMF (solid lines) and by means of three models with the IGIMF, in the case $\beta = 2$ and assuming three different SF efficiencies: $\nu = 0.1$ Gyr^{-1} (dotted lines), $\nu = 0.3$ Gyr^{-1} (dashed lines), and $\nu = 0.5$ Gyr^{-1} (dash-dotted lines), compared to observational data from various authors (see caption of Fig. 6).

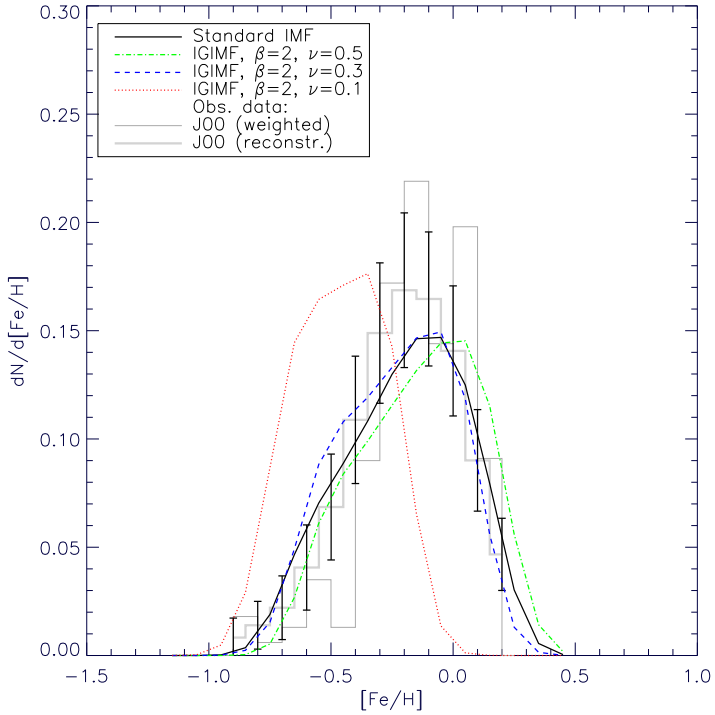

Figure 10. Present-day stellar metallicity distribution in the Solar Neighbourhood. The solid line, the dotted line, the dashed line and the dash-dotted line represent the predicted SMDs computed with the standard IMF, with the IGIMF in the case $\beta = 2$ and SF efficiency $\nu = 0.1$ Gyr^{-1}, $\nu = 0.3$ Gyr^{-1}, and $\nu = 0.5$ Gyr^{-1}, respectively. The histograms are the observational data described in Fig. 7.

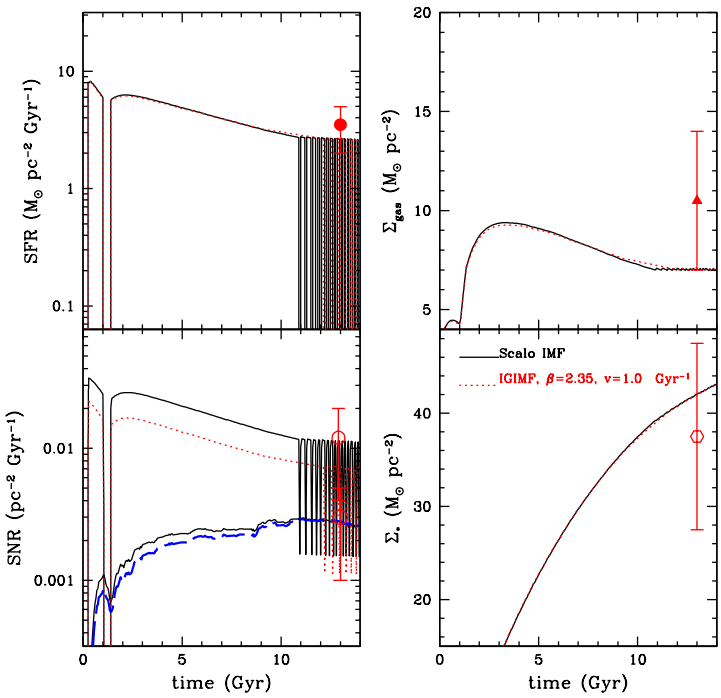

Figure 11. From top-left, clockwise: predicted time evolution of the star formation history, of the gas surface density, stellar surface density and SN rates computed by means of the solar neighbourhhod model with the standard IMF (solid lines) and by means of the best model with the IGIMF, in the case $\beta = 2.35$ and a SF efficiency $\nu = 1$ Gyr^{-1} (dotted lines). In the panel showing the SN rate evolution, the lower and upper curves represent the predicted type Ia and the predicted type II SN rates, respectively. Symbols as in Fig. 5.

can be drawn on the shape of the IMF and on the effects of other parameters such as the SF threshold. The PDMF computed with the standard IMF is in excellent agreement with the observational data in the range 0.4 $M_{\odot}$ - 2 $M_{\odot}$. At stellar masses lower than 0.4 $M_{\odot}$, the standard IMF is too steep and overestimates the observed number of low mass stars. On the other hand, the model computed with the standard IMF underestimates the observed distribution of massive stars with masses $> 30 M_{\odot}$. This is due to the adoption of the SF threshold and its strong effects on the SF history of the solar neighbourhood at late times, inhibiting recent SF and hence causing the underabundance or absence of very massive stars.

The best models calculated with the IGIMF for $\beta = 2$ and $\beta = 2.35$ have different values for the SF efficiencies, but provide all similarly a very good fit to the observed PDMF. The model with $\beta = 1$ slightly underestimates the low-mass end of the PDMF.

The small offsets among the computed distributions are due to different values adopted for the star formation efficiencies. These assumptions produce different values for the present-time stellar mass densities, which reflect into the small offsets visible in Fig. 18.

Our results indicate that the values $\beta = 2$ and $\beta = 2.35$ should be preferred. In the case $\beta = 2.35$, apparently the SF threshold does not affect the computed PDMF. The best model with the IGIMF and $\beta = 2.35$ presents no truncation in the PDMF since, even if the SFR has a gasping behaviour, the frequency of recent star formation events is sufficient to guarantee a significant presence of high-mass stars still living at the present time.

Finally, it is important to stress the importance of the fitness test used to determine which is the best model to reproduce all the obsevables, and how its results depend on the list of observables taken into account. In Table 4, we present our results for the fitness test performed considering (i) the whole set of observables and, for comparison, (ii) computed by considering all observables but the PDMF. In column 1, for each model we report the β values. In column 2, we show the SF efficiencies. In column 3, we show the fitness obtained by using all the obsevables, and in column 4 we present the fitness computed by excluding the PDMF. It is clear that, once the PDMF is excluded and, if one considers the ability to reproduce all the chemical evolution constraints and physical properties such as the SN rates or the gas mass density, the two models with $\beta = 2$, $\nu = 0.3$ Gyr^{-1} and $\nu = 0.5$ Gyr^{-1} are the best, but the standard model provides comparable results. However, the uncapability of the standard model of accurately reproducing the observed PDMF has a strong impact on the fitness computed considering the whole set of observables. In this case, the two models with $\beta = 2$ yield better results than the standard model.

4.9 The time variation of the IGIMF

In Fig. 19, we show how the IGIMF varies as a function of time in the case of the three best models, with $\beta = 2.35$ and $\nu = 2$ Gyr^{-1} (upper panel), with $\beta = 2$ and $\nu = 0.5$

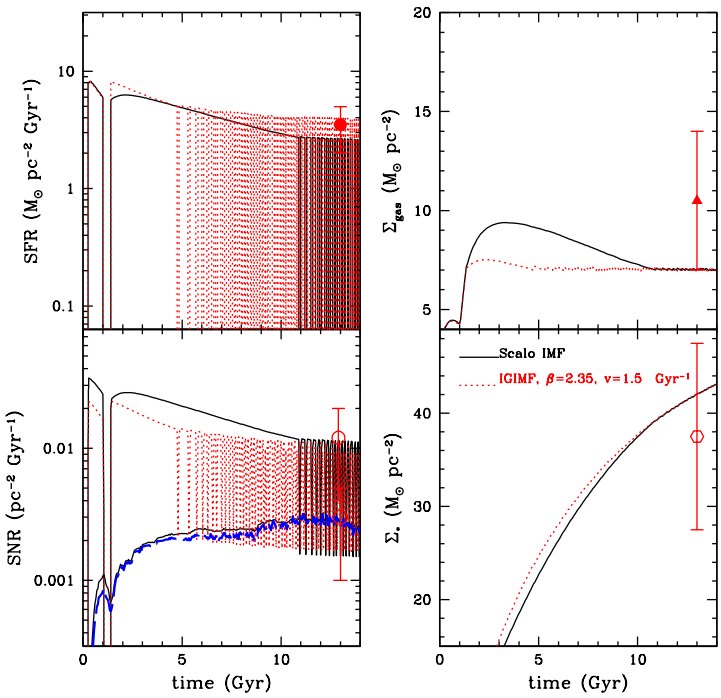

Figure 12. From top-left, clockwise: predicted time evolution of the star formation history, of the gas surface density, stellar surface density and SN rates computed by means of the solar neighbourhhod model with the standard IMF (solid lines) and by means of the best model with the IGIMF, in the case $\beta = 2.35$ and a SF efficiency $\nu = 1.5$ Gyr^{-1} (dotted lines) In the panel showing the SN rate evolution, the lower and upper curves represent the predicted type Ia and the predicted type II SN rates, respectively. Symbols as in Fig. 5.

Gyr^{-1} (central panel) and with $\beta = 1$ and $\nu = 0.1$ Gyr^{-1} (lower panel). In each panel, we show the IGIMF at various epochs, each one characterised by different SFR values.

The best model with $\beta = 1$ is the one characterized by the lowest SF efficiency and presents a rather smooth SFH, although it has stronger variations than the other cases. In fact, as can be seen from Fig. 5, at time 1 Gyr the model with $\nu = 0.1$ Gyr^{-1} has a SFR $< 1 M_{\odot}/yr$, whereas at the present time it has a SFR $\sim 2 M_{\odot}/yr$. On the other hand, in the period going from 1 Gyr to the present time, the other two models have SFR variations within a factor of 2, smaller than in the case with $\nu = 0.1$ Gyr^{-1}. The variations in the SFH of the best model are the cause of the time variations in the IGIMF visible in Fig. 19 at the highest stellar masses ($\log(M/M_{\odot} \sim 1.4)$).

The best model with $\beta = 2$ presents a rather smooth SFR characterised by no strong variation in the period 1 Gyr-14 Gyr (see Fig.8), not influenced by the effects of the star formation threshold. This reflects the very small variation of the IGIMF with cosmic time.
The threshold plays an important role in the evolution of the model with $\beta = 2.35$, whose SFH presents a gasping behaviour throughout the whole cosmic time. As a consequence, the IGIMF presents strong variations.

Our results show that within the IGIMF theory, if the absolute best model reproducing the properties of the solar neighbourhood is the one with $\beta = 2$ and $\nu = 0.5$ Gyr^{-1}, the variation of the IMF with time must be small.

In principle, other objects with extreme variations in the SFH such as starburst galaxies should exhibit a strongly time-varying IMF. This will be an interesting subject for future work.

5 CONCLUSIONS

The initial mass function regulates the number of stars of different intial mass born per stellar generation, hence it plays a fundamental role in galactic chemical evolution studies. The aim of this paper was to test the effects of adopting the integrated galactic initial mass function (IGIMF) on the chemical evolution of the solar neighbourhood. The IGIMF is computed from the combination of the stellar intial mass function, i.e. the mass function in single star clusters, and the embedded cluster mass function, i.e. a power law with index β, and taking into account that within each single cluster, the maximum stellar mass is a function of the total mass of the cluster. The result is a time-varying IMF which is a function of the galactic star formation rate. We applied the formalism developed by Weidner & Kroupa (2005) to a chemical evolution model for the solar neighbourhood, based on the two-infall model by Chiappini et al. (1997). For the embedded cluster mass function, we tested three different values of β and studied various physical quantities and abundances for various chemical elements, comparing our results to the ones obtained by means of a standard IMF, constant in time and similar to the Scalo (1986) IMF. A statistical test to determine which is the best model in reproducing the

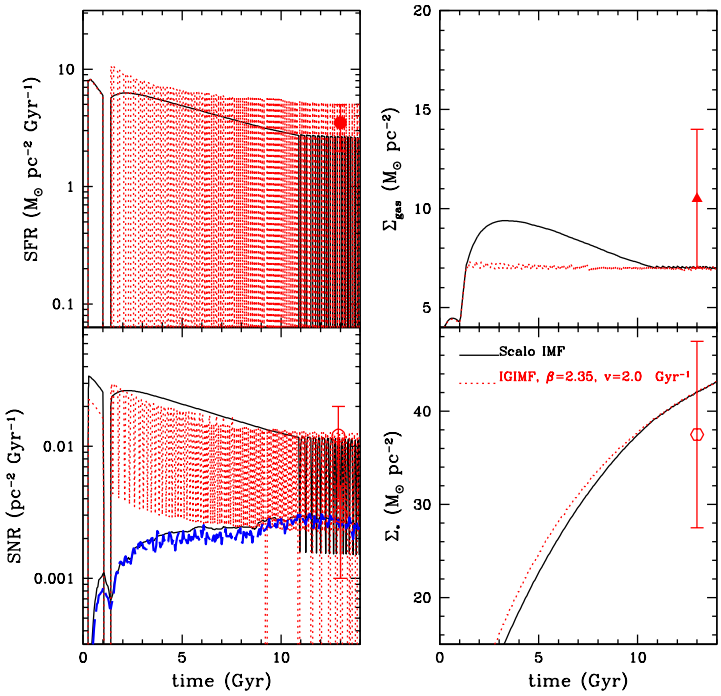

Figure 13. From top-left, clockwise: predicted time evolution of the star formation history, of the gas surface density, stellar surface density and SN rates computed by means of the solar neighbourhhod model with the standard IMF (solid lines) and by means of the best model with the IGIMF, in the case $\beta = 2.35$ and a SF efficiency $\nu = 2$ Gyr^{-1} (dotted lines). In the panel showing the SN rate evolution, the lower and upper curves represent the calculated type Ia and type II SN rates, respectively. Symbols as in Fig. 5.

Table 4. Fitness test for various models in two different cases. In columns 1 and 2, for each model the value of β and SF efficiency values are reported, respectively. In columns 3 and 4, the results of the fitness test computed by considering the whole set of observables and all observables but the PDMF are shown, respectively.

β	ν	Fitness, all observables	Fitness all obs. except PDMF
1.00	0.10	0.54	0.56
1.00	0.25	0.53	0.57
1.00	0.50	0.53	0.55
2.00	0.10	0.47	0.51
2.00	0.30	0.66	0.69
2.00	0.50	0.68	0.72
2.35	1.00	0.48	0.53
2.35	1.50	0.46	0.55
2.35	2.00	0.52	0.55
Standard	1.00	0.56	0.68

set of observational data considered in this work has been developed. Our results can be summarized as follows:
1) The value of β has important effects on the predicted star formation history. Also the effects of the SF threshold may be weaker or stronger, depending on the value chosen for β. In general, lower absolute values of β imply a flatter IGIMF, hence a larger number of massive stars and larger mass ejection rates. This translates into a larger amount of gas available for star formation and gas density values never below the threshold and a smooth star fomation history.
2) The value of β has an obvious deep impact on the predicted SN rates. Beside this, also other quantities can be influenced by this parameter. In general, a lower β implies higher mass ejection rates from massive stars, hence at any time a larger gas mass density.
3) The interstellar abundances are strongly influenced by the parameter β. In general, lower absolute values of β imply higher metallicities and higher [O/Fe] values at a given

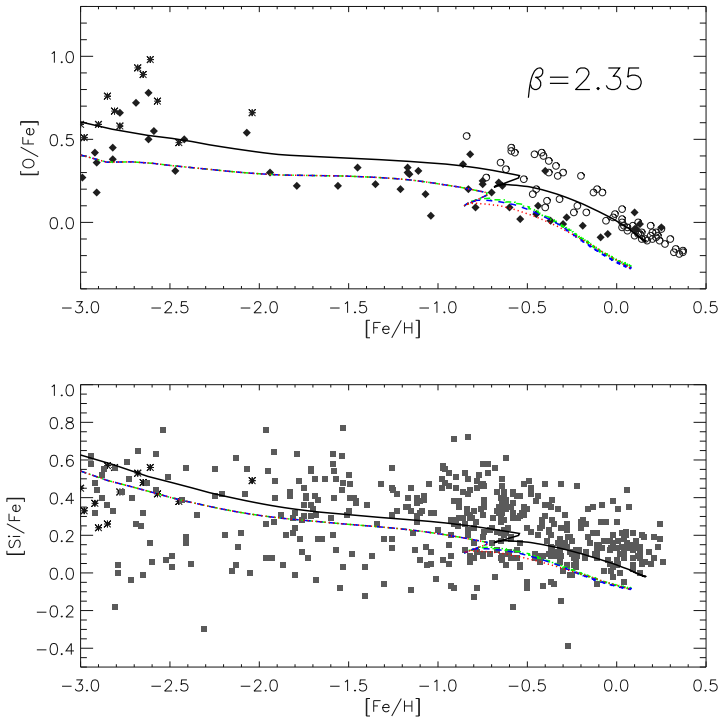

Figure 14. Predicted [O/Fe]-[Fe/H] (upper panel) and [Si/Fe]-[Fe/H] (lower panel) computed by means of the solar neighbourhood model with the standard IMF (solid lines) and by means of three models with the IGIMF, in the case $\beta = 2.35$ and assuming three different SF efficiencies: $\nu = 1$ Gyr^{-1} (dotted lines), $\nu = 1.5$ Gyr^{-1} (dashed lines), and $\nu = 2$ Gyr^{-1} (dash-dotted lines), compared to observational data from various authors (see caption of Fig. 6).

metallicity.

4) We have considered several chemical evolution constraints, including the observed local SN rates, local gas and stellar surface densities, the abundance ratios in local stars and the stellar metallicity distribution and, by varying the SF efficiency, we tested which assumption for the embedded cluster mass function exponent β provides the best simultaneous match to all of these observables. Our fitness test indicates that the best result has been obtained by assuming $\beta = 2$, which produces an IMF resembling that of our standard model and that allows us to account for most of the observables.

5) Useful hints on the initial mass function come from the study of the present day mass function, i.e. the mass function of living stars observed today in the solar neighbourhood. The PDMF is a very good test of the chosen star formation history (Elmegreen & Scalo 2006) once an IMF has been assumed and a valuable test for the IMF once the SFR is assumed. In the case of the standard IMF, the star fomation history assumed here predicts a present-time SFR in good agreement with the observations, and is based on the results by Kennicutt (1989). Models with the IGIMF and different assumptions for β provide different results. Lower values for β produce a PDMF richer in massive stars, whereas higher values of β imply steeper IGIMFs and a lower relative number of massive stars. The model with $\beta = 2$ should be considered the best since it allows to reproduce at the same time the observed PDMF and to account for most of the chemical evolution constraints considered in this work.

In the future, we plan to extend our study of the effects of the IGIMF in galaxies of different morphological types. As forthcoming step, we will investigate how the IGIMF affects the chemical evolution of dwarf galaxies.

ACKNOWLEDGMENTS

We thank C. Chiappini for several interesting discussions.

REFERENCES

Bensby, T.; Feltzing, S.; Lundström, I., 2004, A&A, 415, 155
Boily, C. M.; Kroupa, P., 2003a, MNRAS, 338, 665
Boily, C. M.; Kroupa, P., 2003b, MNRAS, 338, 673
Boissier, S., et al., 2007, ApJS, 173, 524
Calura, F., Matteucci, F., 2006a, ApJ, 652, 889
Calura, F.; Pipino, A.; Chiappini, C.; Matteucci, F.; Maiolino, R., 2009, A&A, 504, 373
Cappellaro, E., 1996, in, eds, Proc. IAU Symp. 171, New Light on Galaxy Evolution. Kluwer Academic, Dordrecht, p.81
Cayrel, R., Depagne, E., Spite, M., et al. 2004, A&A, 416, 1117
Cescutti, G., 2008, A&A, 481, 691
Chabrier, G., 2003, PASP, 115, 763
Chiappini, C., Matteucci, F., Gratton, R. 1997, ApJ, 477, 765
Chiappini, C., Matteucci, F., Padoan, P. 2000, ApJ, 528, 711
Chiappini, C., Matteucci, F., Romano, D., 2001, ApJ, 554, 1044
Chiappini, C.; Romano, D.; Matteucci, F., 2003, MNRAS, 339, 63
Colavitti, E.; Cescutti, G.; Matteucci, F.; Murante, G. 2009, A&A, 496, 429

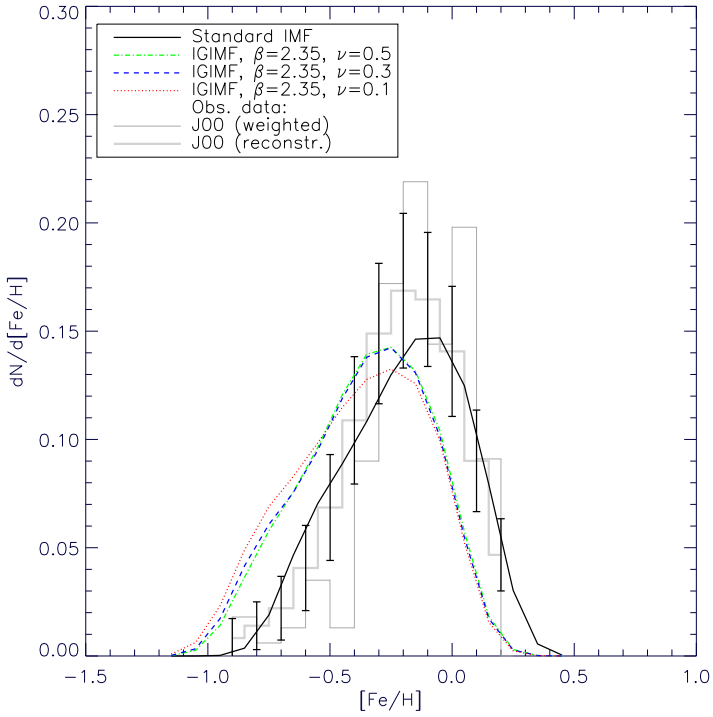

Figure 15. Present-day stellar metallicity distribution in the Solar Neighbourhood. The solid line, the dotted line, the dashed line and the dash-dotted line represent the predicted SMDs computed with the standard IMF, with the IGIMF (in the case $\beta = 2.35$) and SF efficiency $\nu = 1$ Gyr^{-1}, with the IGIMF and SF efficiency $\nu = 1.5$ Gyr^{-1}, and with the IGIMF and SF efficiency $\nu = 2$ Gyr^{-1}, respectively. The histograms are the observational data described in Fig. 7.

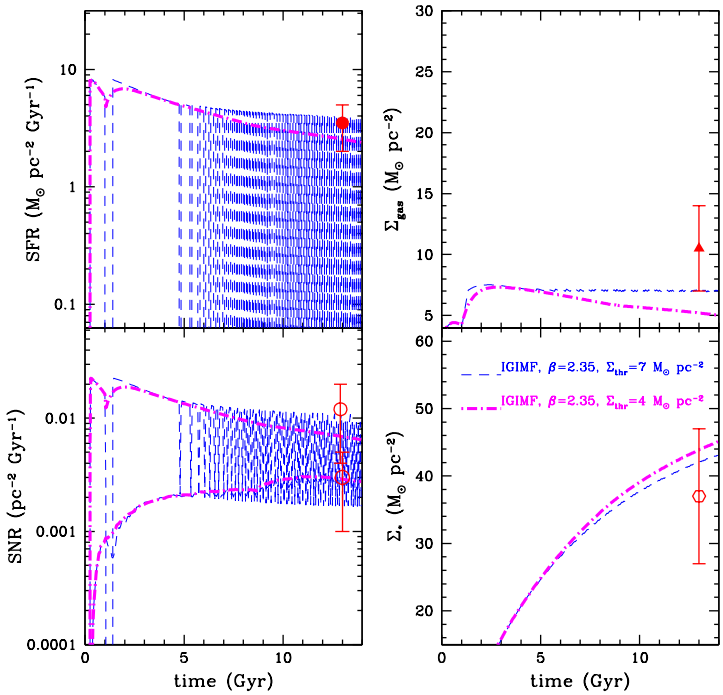

Figure 16. From top-left, clockwise: predicted time evolution of the star formation history, of the gas surface density, stellar surface density and SN rates computed by means of the model with $\beta = 2.35$ and a SF efficiency $\nu = 1.5$ and adopting a SF threshold $\Sigma_{thr} = 7 M_{\odot} pc^{-2}$ (thin dashed lines) and $\Sigma_{thr} = 4 M_{\odot} pc^{-2}$ (thick dot-dashed lines).

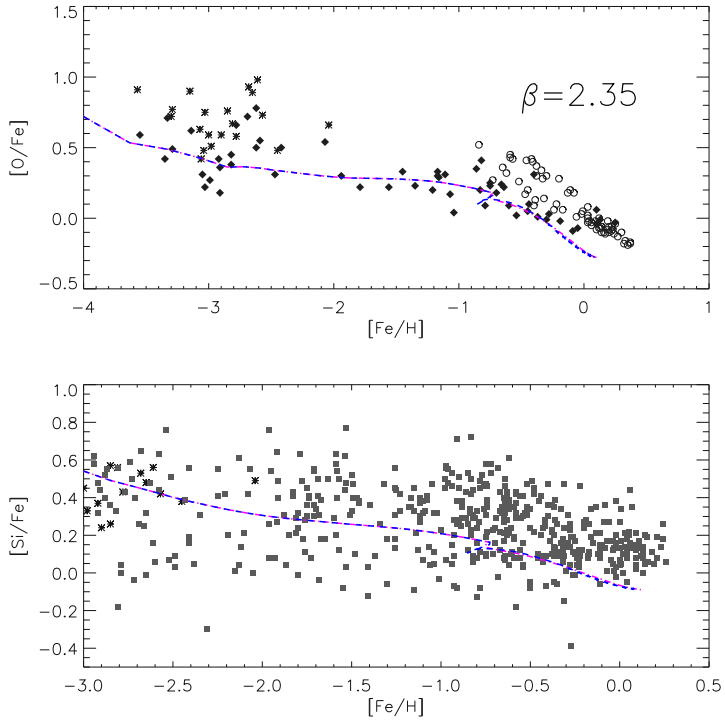

Figure 17. Predicted [O/Fe]-[Fe/H] (upper panel) and [Si/Fe]-[Fe/H] (lower panel) computed by means of the model with $\beta = 2.35$ and a SF efficiency $\nu = 1.5$ and adopting a SF threshold $\Sigma_{thr} = 7 M_{\odot} pc^{-2}$ (dashed lines) and $\Sigma_{thr} = 4 M_{\odot} pc^{-2}$ (thick dot-dashed lines), compared to observational data from various authors.

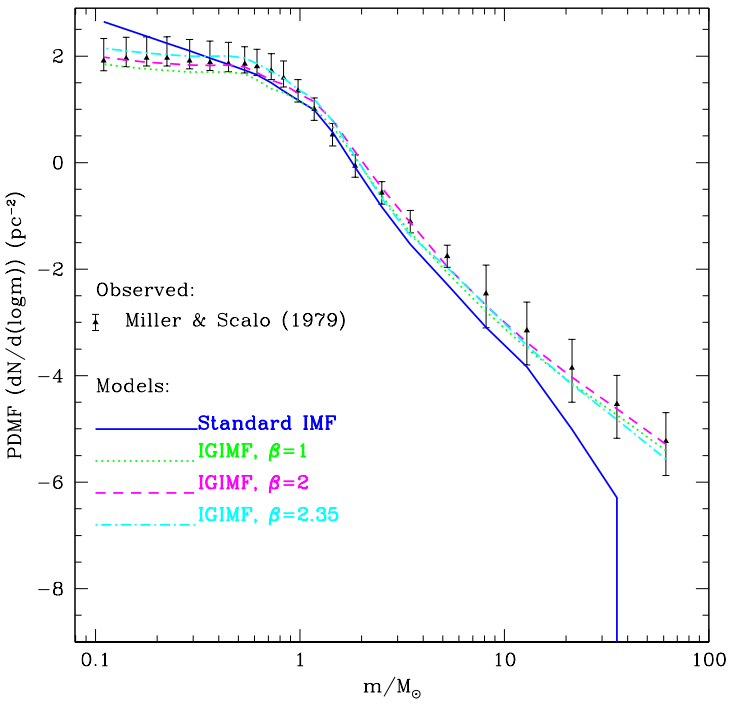

Figure 18. Predicted present-day mass function computed by assuming the standard IMF (thick solid line) and the IGIMF with $\beta = 1$ (thick dotted line), $\beta = 2$ (thick dashed line) and $\beta = 2.35$ (thick dot-dashed line). The observational PDMF is the one of Miller & Scalo (1979) (solid triangles with error bars).

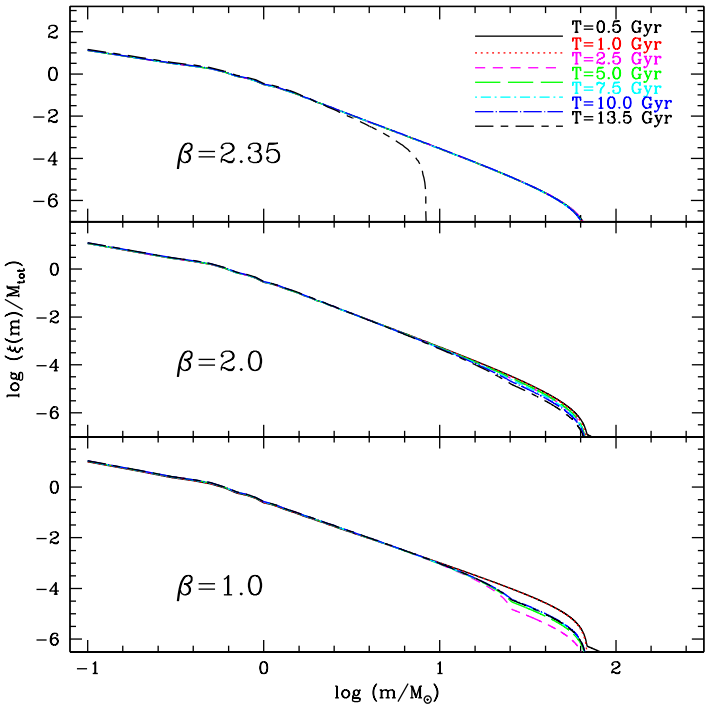

Figure 19. Evolution of the IGIMF as a function of the cosmic time for the models with $\beta = 2.35$ and $\nu = 1.5$ Gyr^{-1} (upper panel), with $\beta = 2$ and $\nu = 0.5$ Gyr^{-1} (central panel) and for the model with $\beta = 1$ and $\nu = 0.25$ Gyr^{-1} (lower panel). In each panel, the curves represent IGIMFs at various times, calculated on the basis of the time variation of the star formation history of each model.

Dame, T. M., 1993, in Holt S. S., Verter F., eds, AIP Conf. Proc. 278, "Back to the Galaxy", Am. Inst. Phys., New York , p. 267

Elmegreen, B. G., Scalo, J., 2006, ApJ, 636, 149

François, F., Matteucci, F., Cayrel, R., et al. 2004, A&A, 421, 613

Gilmore, G., Wyse, R., Kuijen, K., 1989, in "Evolutionary Phenomena in Galaxies", ed. J. Beckman, B. Pagel (Cambridge: Cambridge University Press), 172

Gratton, R., Carretta, E., Matteucci, F., Sneden, C., 2000, A&A, 358, 671

Grevesse, N., Asplund, M., Sauval, A. J. 2007, Space Sci. Rev., 130, 105

Holmberg, J.; Flynn, C., 2004, MNRAS, 352, 440

Israelian, G., Ecuvillo, A., Rebolo, R., et al. 2004, A&A, 421, 649

Iwamoto, K., Brachwitz, F., Nomoto, K., et al. 1999, ApJS, 125, 439

Jorgensen, B. R. 2000, A&A, 363, 947

Kennicutt, R. C., 1989, ApJ, 344, 685

Kennicutt, R. C., 1998, ApJ, 498, 541

Kroupa, P., Weidner, C. 2003, ApJ, 598, 1076

Kroupa, P., Tout, C. A., Gilmore, G. 1993, MNRAS, 262, 545

Kulkarni, S. R., Heiles, C. 1987, in Interstellar Processes, ed. D. Hollenbach, H. Thronson (Dordrecht: Kluwer), 87

Lada, C.J., Lada, E.A., 1991, in Janes K. ed., ASP Conf. Ser. Vol. 13, The Formation and Evolution of Star Clusters, Astron. Soc. Pac. San Francisco, p. 3

Lada, C. J., Lada, E. A. 2003, ARA&A, 41, 57

Larsen, S. S., Richtler, T. 2000, A&A, 354, 836

Larson, R. B. 1976, MNRAS, 176, 31

Martin, C. L.; Kennicutt, R. C., 2001, ApJ, 555, 301

Massey, P., Hunter, D. A. 1998, ApJ, 493, 180

Matteucci, F., François P., 1989, MNRAS, 239, 885

Matteucci, F., Greggio, L., 1986, A&A, 154, 279

Matteucci, F., Recchi, S. 2001, ApJ, 558, 351

Matteucci, F., 2001, ASSL Vol. 253, The Chemical Evolution of the Galaxy. Kluwer, Dordrecht, 293

Matteucci, F., Panagia, N., Pipino, A., Mannucci, F., Recchi, S., Della Valle, M., 2006, MNRAS, 372, 265

Matteucci, F.; Spitoni, E.; Recchi, S.; Valiante, R., 2009, A&A, 501, 531

Méra, D., Chabrier, G., Schaeffer, R. 1998, A&A, 330, 937

Miller, G. E.; Scalo, J. M., 1979, ApJS, 41, 513

Nordström, B., Mayor, M.; Andersen, J.; Holmberg, J.; Pont, F.; Jørgensen, B. R.; Olsen, E. H.; Udry, S.; Mowlavi, N., 2004, A&A, 418, 989

Olling, R. P.; Merrifield, M. R., 2001, MNRAS, 326, 164

Palouš, J., & Theis, C. 2007, A&A, 461, 155

Pflamm-Altenburg, J.; Kroupa, P., 2008, Nature, 455, 641

Pflamm-Altenburg, J., Weidner, C., Kroupa, P. 2007, ApJ, 671, 1550

Rana, N. 1991, ARA&A, 29, 129

Recchi, S.; Calura, F.; Kroupa, P., 2009, A&A, 499, 711

Romano, D., Matteucci, F., Salucci, P., Chiappini, C. 2000, ApJ, 539, 235

Romano, D., Chiappini, C., Matteucci, F., Tosi, M., 2005, A&A, 430, 491

Růžička, A., Palouš, J., Theis, C. 2007, A&A, 461, 155

Salpeter, E. E. 1955, ApJ, 121, 161

Samland, M., Hensler, G., Theis, C. 1997, ApJ, 476, 544

Scalo, J. M., 1986, FCPh, 11, 1

Sommer-Larsen, J.; Götz, M.; Portinari, L., 2003, ApJ, 596, 47

Spite, M., Cayrel, R., Plez, B., et al. 2005, A&A, 430, 655

Talbot, R. J.; Arnett, W. D., 1971, ApJ, 170, 409

Theis, Ch.; Kohle, S., 2001, A&A, 370, 365

Tinsley, B. M. 1980, FCPh, 5, 287

Van den Hoeck, L. B. Groenwegen, M. A. T., 1997, A&AS, 123, 305
Weber, M.; de Boer, W., 2010, A&A, 509, 25
Weidner, C., Kroupa, P. 2005, ApJ, 625, 754
Weidner, C., Kroupa, P. 2006, MNRAS, 365, 1333
Weidner, C., Kroupa, P., Larsen, S.S. 2004, MNRAS, 350, 1503
Whelan, J., Iben, I. Jr. 1973, ApJ, 186, 1007
Zhang, Q., Fall, S. M. 1999, ApJ, 527, L81